# Summertime OH reactivity from a receptor coastal site in the Mediterranean basin

Nora Zannoni[1,*], Valerie Gros[1], Roland Sarda Esteve[1], Cerise Kalogridis[1,2], Vincent Michoud[3,4], Sebastien Dusanter[3], Stephane Sauvage[3], Nadine Locoge[3], Aurelie Colomb[5], Bernard Bonsang[1].

[1] {LSCE, Laboratorie Scientifique du Climat et de l'Environnement, CNRS-CEA-UVSQ, IPSL, Université Paris-Saclay, 91191 Gif sur Yvette, France}

[2] {Institute of Nuclear Technology and Radiation Protection, National Centre of Scientific Research "Demokritos", 15310 Ag. Paraskevi, Attiki, Greece}

[3] {IMT Lille Douai, Univ. Lille, SAGE - Département Sciences de l'Atmosphère et Génie de l'Environnement, 59000 Lille, France}

[4] {Laboratoire Interuniversitaire des Systèmes Atmosphériques (LISA), UMR 7583, CNRS, Université Paris-Est-Créteil et Université Paris Diderot, Institut Pierre Simon Laplace, Créteil, France}

 [5] {LAMP, Campus universitaire des Cezeaux, 4 Avenue Blaise Pascal, 63178 Aubiere, France}

[*] now at: Air chemistry department, Max Planck Institute for Chemistry, Mainz, Germany

Correspondence to: N. Zannoni (norazannoni@gmail.com), V.Gros (valerie.gros@lsce.ipsl.fr)

## Abstract

Total OH reactivity, the total loss frequency of the hydroxyl radical in ambient air, provides the total loading of OH reactants in air. We measured the total OH reactivity for the first time during summertime at a coastal receptor site located in the western Mediterranean basin. Measurements were performed at a temporary field site located in the northern cape of Corsica (France), during summer 2013 for the project CARBOSOR (CARBOn within continental pollution plumes: SOurces and Reactivity) -ChArMEx (Chemistry-Aerosols Mediterranean Experiment). Here, we compare the measured total OH reactivity with the OH reactivity calculated from the measured reactive gases. The difference between these two parameters is termed missing OH reactivity, i.e., the fraction of OH reactivity not explained

by the measured compounds. The total OH reactivity at the site varied between the instrumental LoD (limit of detection= 3 s$^{-1}$) to a maximum of 17±6 s$^{-1}$ (35% uncertainty) and was 5±4 s$^{-1}$ (1σ standard deviation) on average. It varied with air temperature exhibiting a diurnal profile comparable to the reactivity calculated from the concentration of the biogenic volatile organic compounds measured at the site. For part of the campaign, 56% of OH reactivity was unexplained by the measured OH reactants (missing reactivity). We suggest that oxidation products of biogenic gas precursors were among the contributors to missing OH reactivity.

## 1  Introduction

Atmospheric photo-oxidation reactions are initiated by three main oxidants: the hydroxyl radical (OH), ozone (O$_3$) and the nitrate radical (NO$_3$). Among those, the OH radical is by far the most important, capable of reacting with the vast majority of chemical species in the troposphere (Levy, 1971). Photo-oxidation reactions are the most efficient cleansing processes occurring in the atmosphere, and constitute an important sink for reactive gases including volatile organic compounds (VOCs).

Total OH reactivity is the first-order total loss rate of the hydroxyl radical in the atmosphere due to reactive molecules. It is the total sink of OH, therefore representing a top-down measure of OH reactants present in ambient air.

Measurements of the total loss of OH and OH reactive gases are often coupled. The total reactivity of the latter is determined by summing each gas individual reactivity as the product of their atmospheric concentration and their reaction rate coefficient with OH. Here, this is referred to as calculated OH reactivity and comparisons between the calculated and the measured OH reactivity have showed that discrepancies in various environments exist (Di Carlo et al., 2004, Nölscher et al., 2016). The missing OH reactivity, namely the fraction of OH reactivity not explained by simultaneous measurements of reactive gases, has been associated with unmeasured compounds either primary emitted, secondary generated, or both (e.g. Sinha et al., 2010, Nölscher et al., 2012, Nölscher et al., 2013, Edwards et al., 2013, Hansen et al., 2014, Kaiser et al., 2016).

The Mediterranean basin comprises countries from three different continents and a population of 450 million inhabitants. Its climate is characterized by humid-cool winters to hot-dry summers, when the area is usually exposed to intense solar radiation and high temperatures. Forests, woodlands and shrubs occupy large areas of the region, which has rich biodiversity

1    and is the habitat to a high number of identified species (Cuttelod et al., 2008). The dominant

2    airflow in summertime is driven from North to South; therefore, the basin is exposed to air

3    masses coming from European cities and industrialized areas. Transported pollution and the

4    intense local anthropogenic and biogenic activity result in high loadings of atmospheric gases,

5    particles and complex chemistry (Lelieveld, 2002).

6    Climate model predictions indicate that the Mediterranean area will face unique impacts of

7    climate change. Predictions show that this region will suffer higher temperatures and

8    extended drought periods, thus affecting the strength and type of emissions which will further

9    impact air quality and climate (Giorgi and Lionello, 2008). Finally, additional observations

10   are useful for better predicting the future state of this region (Mellouki and Ravishankara,

11   2007).

12   In this study, we address the following scientific questions:

13      1) What proportion of the total reactive gases emitted and formed over the area do we

14         know and can we detect?

15      2) Which species mostly influence the OH reactivity over this site within the basin?

16   To answer these questions, we measured the total OH reactivity at a receptor coastal site in

17   the western Mediterranean basin during summer 2013. Measurements were part of an

18   intensive fieldwork campaign aimed at investigating sources and sinks of gaseous constituents

19   in the area (CARBOSOR, carbon within continental pollution plumes: Sources and

20   Reactivity, within the ChArMEx project, Chemistry and Aerosols in a Mediterranean

21   Experiment; charmex website: http://charmex.lsce.ipsl.fr/). We measured the total OH

22   reactivity with the comparative reactivity method instrument (CRM) (Sinha et al., 2008)

23   during 16/07/2013-05/08/2013 at the monitoring station of Ersa, France. The field site was

24   chosen for being: (i) far from anthropogenic sources; (ii) exposed to aged air masses of

25   different origins, including air masses enriched in oxidation products transported from

26   continental industrialized areas. Total OH reactivity here served to evaluate whether the

27   ambient reactive gases were all identified or not. Specifically, it was useful to determine what

28   kind of pollution event could be better captured through the instrumentation deployed at the

29   site, assuming that a group of reactive gases traces a specific type of event (primary

30   anthropogenic or biogenic emissions, secondary formation). Due to the high number of

31   existing VOCs, OH reactivity also makes a powerful means for investigating VOC emissions

32   and reactions. The following sections will describe the field site under study, the

1 methodologies used, our results of OH reactivity and insights into the unmeasured reactive

2 gases.

## 2 Field site

4 The Ersa windfarm (42.97°N, 9.38°E, altitude 533 m) is located in the northern cape of

5 Corsica (France), in the western Mediterranean basin (Figure 1). It is 2.5 km away from the

6 nearest coast (West side) and 50 km away from the largest closest city and harbour Bastia

7 (South side). It is located on a hill (533 m a.s.l.) and it is surrounded by the Mediterranean Sea

8 on West, North and East sides. The site is exposed to air masses from continental areas

9 especially France and northern Italy, with the harbours of Marseille and Genoa about 300 km

10 away, and the industrialized areas of Milan and the Po valley 400 km away. Furthermore, the

11 Mediterranean maquis, a shrubland biome typical of the Mediterranean region, densely

12 surrounds the measurement station. The ground station consists of a long-term meteorology,

13 trace gas concentrations, aerosol size and composition monitoring laboratory (measurements

14 collected from 2012 to 2014), and temporary measurements of gases and aerosol properties

15 over a total surface area of ~100 $m^2$ where instruments are distributed. Measurements of total

16 OH reactivity and trace gases reported in this study were all performed within this area (see

17 Figure 1 for details).

18 We measured the OH reactivity during two main periods: an intercomparison exercise for OH

19 reactivity between two CRM instruments during 8/07/2013-13/07/2013 (see Zannoni et al.,

20 2015), and the intensive ambient monitoring campaign, CARBOSOR during 16/07/2013-

21 05/08/2013. Within the same project, instruments for measuring radicals, inorganic and

22 organic compounds, aerosol chemical composition and physical properties, and meteorology

23 were simultaneously deployed. The next section will provide an overview of the methods

24 selected for this study.

## 3 Methods

### 3.1 Comparative Reactivity Method

27 We carried out measurements of total OH reactivity using a comparative reactivity method

28 instrument assembled in our laboratory (CRM-LSCE from Laboratoire des Sciences du

29 Climat et de l' Environnement, see Zannoni et al., 2015). In brief, the comparative reactivity

30 method is based on the concept of producing a competition for in-situ generated OH radicals,

31 between a reactive reference compound, in our case pyrrole ($C_4H_5N$), and ambient reactive

1    gases (Sinha et al., 2008). This is achieved by introducing a known amount of pyrrole diluted

2    in zero air and $N_2$ in a flow reactor coupled to a Proton Transfer Reaction-Mass Spectrometer

3    (PTR-MS, see Lindinger et al., 1998, De Gouw and Warneke, 2007). Pyrrole is chosen as a

4    reference compound for its well characterized kinetics (Atkinson et al., 1984, Dillon et al.,

5    2012), for not being present in the atmosphere at normal conditions, and for being easily

6    detectable at the protonated *m/z* 68 ($C_4H_5NH^+$) through PTR-MS without any interference.

7    The Proton Transfer Reaction-Mass Spectrometer run at standard conditions (Pdrift = 2.2

8    mbar, E/N = 130 Td (1 Td=$10^{-17}$ Vcm$^{-1}$), Tinlet = 60 ∘C) is the detector of choice for its real-

9    time measurement capabilities and robustness over time (see also Nölscher et al., 2012b).

10    The CRM usual experimental procedure includes the following stages: monitoring of C0

11    wet/dry, followed by C1 dry or wet, C2 wet, and C3 ambient. With C0, C1, C2, C3 being the

12    concentration of pyrrole detected with the PTR-MS, in order: after injection (C0), after

13    photolysis of pyrrole (C1), after reaction with OH (C2), when ambient air is injected and the

14    competition for OH radicals starts (C3). Switches between C2 (background pyrrole in zero

15    air) and C3 (pyrrole in ambient air) result in modulations of the pyrrole signal, which are used

16    to derive total OH reactivity values from the following equation:

17

18    $$R_{air} = \frac{(C3-C2)}{(C1-C3)} \cdot k_{pyrrole+OH} \cdot C1 \qquad\qquad (1)$$

19    With $k_{pyrrole+OH}$ being the rate constant of reaction between pyrrole and OH=

20    $(1.20\pm0.16)\times10^{-10}$ cm$^3$ molecule$^{-1}$ s$^{-1}$ (Atkinson et al., 1984, Dillon et al., 2012).

21    During the whole campaign, we ran systematic quality check controls on the instrument (see

22    supplementary material).

23    Sampling was performed through a 3 m long, 1/8'' OD PFA sampling line at a flow rate of

24    0.25 sL/min with a residence time of the sample of 3 s. The sampling line was covered and

25    kept at ambient temperature and installed at about 1.5 m above the trailer were the CRM was

26    installed. A PFTE filter was placed at the inlet of the sampling line to avoid sampling

27    particles. Some highly-reactive chemical species (i.e. sesquiterpenes) may have been lost

28    before reaching the reactor due to wall losses in the sampling line and/or filter surface.

29    We recorded PTR-MS data using a dwell time of 20 s for pyrrole, with a full cycle of

30    measurements every 30 s. We switched between C2 and C3 every 5 minutes, resulting in a

31    data point of reactivity every 10 minutes. Each data point of reactivity obtained from eq. (1)

was corrected for: (i) humidity changes between C2 and C3, (ii) deviation from the assumption of pseudo fist order kinetics between pyrrole and OH, (iii) dilution of ambient air reactivity inside the reactor. A detailed description on how the correction factors were obtained and how the raw data were processed can be found in the publication of Zannoni et al., (2015). We did not account for OH recycling in our reactor due to nitrogen oxides (NO+ $NO_2$) since ambient nitrogen monoxide (NO) was below 0.5 ppbv at the site ($NO_2$ below 2 ppbv), which is too low for interfering with the system. Tests performed in the laboratory after the campaign have demonstrated that the instrument is not subject to ozone interference. The impact on CRM measurements of OH recycling reactions observed during the oxidation of some ambient species (e.g. methylvinylketone and methacrolein (MVK+MACR), isoprene hydroxyhydroperoxides (ISOPOOH), aldehydes) was determined to be negligible due to the low concentrations of these species and the high $HO_2$ concentration in the CRM reactor, which disfavor unimolecular reactions.

The limit of detection (LoD) of CRM-LSCE was estimated to be ~3 $s^{-1}$ (3σ) and the systematic uncertainty ~35% (1σ), including uncertainties on the rate coefficient between pyrrole and OH (8%), detector sensitivity changes and pyrrole standard concentration (22%), correction factor for kinetics regime (26%) and flows fluctuations (2%); see also Michoud et al., 2015. An intercomparison exercise with another CRM instrument carried out before the campaign demonstrated that the measured reactivities were in good agreement (linear least squares fit with a slope of one and $R^2$ value of 0.75).

## 3.2   Complementary measurements at the field site

Trace gases were measured using a broad set of techniques available at the site, including: Proton Transfer Reaction-Mass Spectrometry (PTR-Time of Flight MS, Kore Technology Ltd., UK), online and offline Gas Chromatography (GC-FID/FID and GC-FID/MS, Perkin Elmer), Liquid Chromatography (HPLC-UV, High Performance Liquid Chromatography-UV light detector), the Hantzsch reaction method (AERO-LASER GmbH, Germany) and wavelength-scanned cavity ring down spectrometer (WS-CRDS, G2401, Picarro, USA). The measured concentration and the reaction rate coefficients of each measured compound with OH were used to calculate the OH reactivity with eq. (2):

$$R = \sum_i k_{i+OH} \cdot X_i \tag{2}$$

With $i$ being any measured compound listed in Table 1 and X its concentration.

Most of the chemical species whose reactivity was summed to determine the calculated reactivity were measured through PTR-MS and GC.

The sampling system for the PTR-MS consisted of a 5 m PFA sampling line, installed above the PTR-MS trailer (see Figure 1). The residence time in the sampling line was 4 s. We operated the PTR-MS at 1.33 mbar pressure and 40°C temperature in the drift tube for an E/N of 135 Td. The PTR-MS was calibrated every 3 days using certified mixtures of different VOCs: 15 VOCs (Restek, France), 9 VOCs (Praxair, USA), 9 OVOCs (Praxair, USA). More details on the calibration standards are available in Michoud et al. (2017). For this campaign, we only reported the masses that we clearly identified and for which we had a calibration standard. Some other masses, possibly corresponding to oxidation products of terpenes were also extracted from the mass spectra and tentatively quantified (e.g. *m/z* 99, 111, 113, 155). A visual inspection of the full mass spectra did not reveal any other abundant species that we did not consider. The GCs were calibrated twice at the beginning and at the end of the field campaign with certified gas mixtures: one including 29 VOCs (Praxair, USA), another including 29 NMHCs and three terpenes (NPL, UK). Total uncertainties from measurements (including precision and calibration procedure) were in the range 5-23% for compounds measured by PTR-MS and GC-FID, and in the range 5-14% for GC-MS.

Isoprene was measured by both PTR-MS and GC and the results correlated within the measurement uncertainty (slope and $R^2$ of the regression for 415 data points are 0.93±0.03 and 0.77, respectively; see supplement). A small offset in the scatter plot (approximately 100 pptv) may indicate a small interference at *m/z* 69 for the PTR-MS measurements; therefore, we used data from GC to calculate the OH reactivity. We sampled individual monoterpenes with GC-FID, and on adsorbent tubes for the analysis with GC-MS, while we measured the total monoterpenes fraction by PTR-MS since the instrument cannot distinguish between structural isomers. Concentrations obtained from GC techniques were used to calculate the summed OH reactivity. As recently reported by Rivera-Rios et al., 2014, the *m/z* 71 measured by PTR-MS might also include the ISOPOOH which could have formed at the site and fragmented inside the PTR-MS. However, it is important for the reader to know that we did not separate the different components of the *m/z* 71, therefore the presence of ISOPOOH on *m/z* 71 is assumed based on the recent literature.

We refer to the manuscript of Michoud et al.(2017), for a detailed description of the PTR-MS, online GC and offline sampling on adsorbent cartridges on GC-FID/MS deployed at the site;

1 while the formaldehyde, $NO_x$, $O_3$ analysers and WS-CRDS are briefly introduced in the
2 following sections. Table 2 provides a summary of all techniques.

3 3.2.1 Hantzsch method for measuring formaldehyde

4 Formaldehyde (HCHO) was measured with a commercial instrument based on the Hantzsch
5 reaction (Model 4001, AERO-LASER GmbH, Germany). Gaseous HCHO is stripped into a
6 slightly acidic solution, followed by reaction with the Hantzsch reagent, i.e. a diluted mixture
7 of acetyl acetone acetic acid and ammonium acetate. This reaction produces a fluorescent
8 compound, which absorbs photons at 510 nm. More details are given in Dasgupta et al.,
9 (1988), Junkermann, (2009) and Preunkert et al., (2013).

10 Sampling was conducted through a 5 m long PTFE 1/4'' OD line, with a 47 mm PFA in-line
11 filter installed at the inlet and a flow rate of 1 L $min^{-1}$.

12 The liquid reagents (stripping solution and Hantzsch reagent) were prepared from analytical
13 grade chemicals and ultrapure water according to the composition given by Nash, (1953) and
14 stored at 4 °C on the field. The instrumental background was measured twice a day (using an
15 external Hopcalite catalyst consisting of manganese and copper oxides) and calibrated three to
16 four times a week using a liquid standard at $1.10^{-6}$ mol $L^{-1}$, i.e volume mixing ratio in the
17 gaseous phase of about 16 ppbv. The calibration points were interpolated linearly in order to
18 correct for sensitivity fluctuations of the instrument. The limit of detection was 130 pptv ($2\sigma$).
19 The coefficient of variation, i.e the ratio of the standard deviation to the mean background
20 value, was estimated to be 0.4 %. Measurements of HCHO ran smoothly from the beginning
21 of the campaign until 11 AM LT (local time) of 28/07/2013. At this time, an instrument
22 failure occurred and measurements were stopped.

23 3.2.2 Chemiluminescence for measuring $NO_x$

24 A CRANOX instrument (Ecophysics, Switzerland) based on ozone chemiluminescence was
25 used to measure nitrogen oxides ($NO_x$=NO+$NO_2$). Nitric oxide is quantified directly by the
26 instrument while $NO_2$ is quantified indirectly after being photolytically converted to NO
27 (conversion efficiency=86%). The instrument consists of a high performing two channel
28 CLDs (Chemiluminescence Detectors) with pre-chambers background compensation, an
29 integrated pump, a photolytic converter, an ozone generator and a calibrator. A control
30 software handles and manages the different tasks. The detection limit is 50 pptv ($3\sigma$), and the
31 time resolution is 5 minute.

1  3.2.3 Wavelength-scanned cavity ring down spectrometry (WS-CRDS) for measuring

2  greenhouse gases

3  In-situ measurements of $CO_2$, $CH_4$, CO molar fractions at Ersa are part of the French

4  monitoring network of greenhouse gases, integrated in the European Research Infrastructure

5  ICOS (integrated carbon observation system). The air is sampled at the top of a 40 m high

6  telecomunication tower (573 m), and is analyzed with a wavelength-scanned cavity ring down

7  spectrometer (WS-CRDS, G2401, Picarro, USA). The analyzer is calibrated every 3 weeks

8  with a suite of four reference standard gases, whose molar fractions are linked to the WMO

9  (World Meteorological Organization) scales through the LSCE (Laboratoire des Sciences du

10  Climat et de l'Environnement) reference scale. Measurements were corrected for an empirical

11  correction which takes into account the dilution effect and pressure broadening effect. A

12  humidifying bench was developed to humidify a certified concentration of a gas stream at

13  different humidity levels (see Rella et al., 2013).

14  **3.3   Air masses back-trajectories**

15  The back-trajectories of the air masses were modelled with Hysplit (HYbrid Single-Particle

16  Lagrangian Integrated Trajectory developed by the National Oceanic and Atmosphere

17  Administration (NOAA) Air Resources Laboratory (ARL) (Draxler and Hess, 1998, Stein et

18  al., 2015) for 48 h every 6 hours.

19  The back-trajectories were grouped according to their origin, altitude and wind speed, such

20  as: 1.North-East, 2.West, 3.South, 4.North-West and 5. Calm-low wind speed/stagnant

21  conditions. More details on the air masses origin and their photochemical age is available in

22  Michoud et al., (2017).

23  **4   Results**

24  **4.1   Total measured OH reactivity**

25  The black line in Figure 2 represents the 3-h averaged measured OH reactivity. Here we

26  report all data acquired during 16/07/2013- 05/08/2013, missing data points are due to minor

27  instrumental issues and instrumental controls. Figure 2 also shows the temperature profile of

28  ambient air (gray line, right axis). The OH reactivity varied between the instrumental LoD (3

29  $s^{-1}$) to 17±6 $s^{-1}$ (3-h averaged maximum value ± 35% uncertainty). From the 10 minute time

30  resolution data the highest value of OH reactivity was 22 $s^{-1}$, reached on 28/07/2013 during

the afternoon, when the air temperature at the site was also exhibiting its maximum. During the whole field campaign, the average measured OH reactivity was $5\pm4$ s$^{-1}$ (1σ). This value agrees with averaged values of OH reactivity collected during autumn 2011 in the South of Spain for southernly marine enriched air masses (Sinha et al, 2012). In contrast, higher OH reactivity was measured during spring 2014 in a Mediterranean forest of downy oaks, where the average campaign value was $26\pm19$ s$^{-1}$ and the maximum value was 69 s$^{-1}$ (Zannoni et al., 2016).

Hydroxyl radical reactivity and air temperature at the site in Corsica co-varied during the whole campaign, with highest values reached during daytime in the periods between July 26-28 and August 2-3. In Figure 2 the origin of the air masses reaching the field site is also reported. The dominant origin of the sampled air masses was west, indicating air masses that had travelled over the sea being possibly more aged. It is not evident that the variability of the OH reactivity is affected by the origin of the air masses; in contrast, air temperature seems to have played a major role. The diurnal pattern of OH reactivity for the whole campaign is reported in Figure 3. Here it is evident that the background value was about 4 s$^{-1}$ during nighttime, it increased at 8:00 AM LT, peaked at 11:00 AM LT, reached a second maximum at 4:00 PM LT and finally decreased at 7:00 PM LT to reach its background value at 10:00 PM LT (local time GMT/UTC+2 hours). It is worth noting that the large amplitude of standard deviation bars (1σ) highlights the large diel variability.

## 4.2 Calculated OH reactivity and BVOCs influence

Table 1 provides the number and type of chemical species measured simultaneously with the OH reactivity. We determined the calculated OH reactivity from the concentrations and reaction rate coefficients with OH of the species reported in Table 1 using eq. (2). Please refer to Table 2 in the supplementary material for the reaction rate coefficients of the selected compounds with OH. A broad set of compounds were monitored at the site, herein classified as: anthropogenic volatile organic compounds (AVOCs, 41 compounds measured), biogenic volatile organic compounds (BVOCs, 7), oxygenated volatile organic compounds (OVOCs, 15) and others (3 species: CO, NO and NO$_2$). Please notice that this classification was adopted to simplify the discussion throughout the manuscript, for more details concerning the different sources of these compounds the reader can refer to the notes of Table 1. Figure 2 shows the time series of the summed calculated OH reactivity (thick blue line) and the

contributions of each class of chemicals. The maximum of the summed calculated OH reactivity was 11 s$^{-1}$, and the 24-h averaged value was 3±2 s$^{-1}$ (1σ). As represented in Figure 3, the class of the biogenic compounds played an important role on the daytime OH reactivity. Here, the shape of the diurnal pattern of the measured reactivity is slighty shifted to the BVOCs OH reactivity, which suggests a possible influence from the oxidation products of biogenic molecules. The mean percentage contribution of each class of compounds to the summed calculated reactivity is determined for daytime (from 07:30 to 19:30, LT) and nighttime data (from 19.30 to 04.30 LT) in Figure 4. During daytime BVOCs contributed the largest fraction of OH reactivity (45%), followed by inorganic species (24%), OVOCs (19%) and AVOCs (12%). Interestingly, only 7 BVOCs had a higher impact than 41 AVOCs. This is explained by: i) the relatively high concentration of BVOCs (maximum values for isoprene and sum of monoterpenes is 1 and 1.5 ppbv, respectively), ii) the generally large BVOC reaction rate coefficients with OH (Atkinson and Arey, 2003) and iii) the relatively low concentration of AVOCs measured during the campaign. BVOCs accounted only for 5% of the total VOCs concentration, followed by AVOCs (15%) and OVOCs (79%) (mean campaign values, see also Michoud et al., 2017) which highlights the reactive nature of the measured BVOCs. During nighttime, BVOCs concentrations decreased (see Figures 2 and 3); CO and NO$_x$ had the largest influence on OH reactivity (43%), followed by OVOCs (27%), AVOCs (23%) and BVOCs (7%). Particularly, CO and long-lived OVOCs and AVOCs constituted a background reactivity of ~ 2-3 s$^{-1}$, as also shown by the diurnal profiles reported in Figure 3.

Inside the BVOCs class, the total fraction of monoterpenes contributed more than isoprene to the OH reactivity (Figure 5). During daytime, OH reactivity due to monoterpenes was between 1.4 to 7.4 s$^{-1}$ and varied with air temperature, on the other hand, isoprene reactivity with OH varied between 0.3-2.3 s$^{-1}$ (minimum and maximum values on 29/07/13 and 03/08/2013, respectively). In contrast with monoterpenes OH reactivity, the reactivity of isoprene towards OH varied with both air temperature and solar irradiance. Overall, both monoterpenes and isoprene OH reactivities had the characteristic diurnal profile observed for their atmospheric concentrations. High concentrations depended on air temperature, solar radiation as well as calm-low wind speed conditions. These results indicate a large impact of BVOC oxidation on the local photochemistry.

1　The very reactive monoterpene α-terpinene had the largest contribution on OH reactivity

2　among the measured BVOCs (31%), followed by isoprene (30%), β-pinene (17%), limonene

3　(12%), α-pinene (8%), camphene (2%) and γ-terpinene (1%), over a total averaged daytime

4　reactivity due to BVOCs of 2±2 s$^{-1}$ (1σ), see Table 3. During the night, monoterpenes had a

5　larger impact than isoprene due to their known temperature dependency (Kesselmeier and

6　Staudt, 1999). α-terpinene was the most reactive-to-OH BVOC also during nighttime, see

7　Table 3. In terms of absolute values, α-terpinene had a maximum reactivity of 5.3 s$^{-1}$ on the

8　2$^{nd}$ of August at 2:00 PM LT, which is also when the maximum OH reactivity reported for the

9　whole class of BVOCs occurred. Remarkably, the mean concentration of this compound made

10　it the fourth most abundant BVOC measured, with isoprene being the first (35%), followed by

11　β-pinene (22%), α-pinene (15%), α-terpinene (13%), limonene (9%) and γ-terpinene (1%).

12　The α-terpinene volume mixing ratio was maximum 594 pptv, with an average value between

13　10:00 AM LT and 5:00 PM LT during the field campaign of 131±110 pptv. Its short lifetime

14　is due to the high reaction rate coefficient towards OH, (as reported in literature, i.e. $3.6 \times 10^{-10}$

15　cm$^3$ molecule$^{-1}$ s$^{-1}$, see Atkinson, (1986) and Lee et al., (2006)), which is more than three-fold

16　higher than the one of reactive isoprene ($k_{isoprene+OH} = 1 \times 10^{-10}$ cm$^3$ molecule$^{-1}$ s$^{-1}$, Atkinson,

17　1986). Very little is reported in literature regarding its emission rates and ambient levels in the

18　Mediterranean region. Owen et al., (2001) measured α-terpinene from a few Mediterranean

19　tree species, including: *Juniperus phoenicea, Juniperus oxycedrus, Spartium junceum L., and*

20　*Quercus ilex.* Ormeno et al., (2007) published the α-terpinene content as 34.9±2.3 μg/gDM in

21　the leaves of *Rosmarinus officinalis*; shrubs of rosemary were present in large quantity around

22　our field site in Corsica.

23　**4.3　Missing reactivity and air masses fingerprint**

24　Figure 2 reports the time series of the total measured OH reactivity and calculated OH

25　reactivity with their associated errors (35% and 20%, respectively). The largest significant

26　discrepancy between reactivities occurred during July 23-30 (56% of missing reactivity on

27　average). We combined air mass backtrajectories and atmospheric mixing ratios of some

28　common atmospheric tracers to determine the chemical fingerprint of the sampled air and to

29　investigate the origin of the missing reactivity. We chose isoprene and pinenes for air masses

30　influenced by biogenic activity, while propane and CO were used for those enriched in

31　anthropogenic pollutants (see supplement). Maximum concentrations of anthropogenic

32　pollutants were measured when the air masses originated from the North East sector: between

July 21-23 and between July 31 and August 3, indicating weak pollution events coming from the industrialized areas of the Po Valley and Milan (Italy). On the other hand, biogenic activity was independent of the wind sector and showed some variability linked to local drivers, such as the air temperature, solar irradiance and wind speed (Figure 6). Remarkably, measured OH reactivity and missing OH reactivity showed no dependency on the origin of air masses.

## 4.4 Insights into the missing OH reactivity

The missing OH reactivity, defined as the absolute difference between measured and calculated reactivity values, is reported in Figure 6. Only values higher than the detection limit of 3 s$^{-1}$ are displayed in this figure. Significant missing reactivity (2.8±2.2 s$^{-1}$ on average over the whole campaign) can be observed during 23 to 29 July and more sporadically before 23 July (3 data points over a total of 41) and after 29 July (10 data points). To determine the causes of the reported missing OH reactivity we first investigated whether the instruments did not selectively detect primary-emitted BVOCs. We compared the total monoterpene concentration observed by PTR-MS to the summed monoterpenes concentration from GCs and calculated a concentration difference ranging from 0.2 to 0.6 ppbv (see supplement), the PTR-MS measurements being higher than the sum of speciated monoterpenes. Assuming a reaction rate coefficient with OH of $1.56 \times 10^{-10}$ cm$^3$ molecule$^{-1}$ s$^{-1}$ (weighted value estimated from monoterpenes emitted by the plants present at the site, see Bracho-Nunez et al., 2011) we can roughly estimate a value of 0.8-2.3 s$^{-1}$ of missing OH reactivity, which is only 30% the reported missing reactivity on average. Therefore, unmeasured monoterpenes account for a significant fraction of the missing OH reactivity but do not fully explain the total missing budget.

The missing OH reactivity temperature dependency was used in previous studies (Di Carlo et al, (2004), Mao et al., (2012) and Hansen et al., (2014)) to determine whether terpenes (Di Carlo et al., 2004) or their oxidation products (Mao et al., 2012) could explain the missing OH reactivity. Terpenes emissions depend on temperature following the expression, $E(T)$ =$E(Ts)\exp[\beta(T - Ts)]$, where $E(Ts)$ is the emission rate at temperature $Ts$, $\beta$ a temperature sensitivity factor and $T$ the ambient temperature. Di Carlo et al., (2004) found that the missing OH reactivity reported from a temperate forest in northern Michigan followed the same temperature dependency as terpene emissions, with $\beta= 0.11$ K$^{-1}$. Similarly, Mao et al., (2012) reported a $\beta$ factor of 0.168 K$^{-1}$ from a temperate forest in California. Since this value is

1  higher than the upper limit of 0.144 usually observed for terpene emissions, the authors

2  attributed the missing OH reactivity to unmeasured oxidation products of BVOCs and they

3  confirmed it with box model simulations.

4  In the present study, we found a clear dependence ($\beta$= 0.158 K$^{-1}$ and R$^2$=0.643) between the

5  missing OH reactivity and temperature for some days of the campaign (27th, 28th, 29th), while

6  no correlation ($\beta$= 0.007 K$^{-1}$ and R$^2$=0.001) was found during 23-26 July, see Figure 7. The

7  similarity with the sensitivity coefficient from the study of Mao et al., (2012) and the diurnal

8  profile observed for the missing reactivity indicate that BVOC oxidation products might have

9  contributed to the missing reactivity observed during July 27-28-29.  In contrast, the lack of a

10  temperature dependence for the 23-26 July period indicates that species other than BVOC

11  oxidation products locally formed may have played a role in the missing OH reactivity.

12  Figure 6 shows the missing OH reactivity and volume mixing ratios of BVOCs and their

13  oxidation products together with local atmospheric conditions, such as temperature, wind

14  speed and solar irradiance. Compounds are reported using their protonated mass measured by

15  PTR-MS, such as: *m/z* 69 (isoprene) and *m/z* 137 (monoterpenes) for primary emissions, *m/z*

16  71 (isoprene first generation oxidation products: Methyl Vinyl Ketone (MVK) + methacrolein

17  (MACR) + possibly isoprene hydroxyperoxides (ISOPOOH)), *m/z* 139 (nopinone, $\beta$-pinene

18  first generation oxidation product) and *m/z* 151 (fragment of pinonaldehyde, $\alpha$-pinene first

19  generation oxidation product) for the BVOC oxidation products.  It is worth noting that *m/z*

20  111 and *m/z* 113 are also reported since these masses have been attributed to oxidation

21  products of several terpenes. Indeed *m/z* 111, *m/z* 113 and *m/z* 151 were observed in chamber

22  and field studies (Lee et al., 2006, Holzinger et al., 2005) as they are formed from the photo-

23  oxidation of different terpenes; highest yields were attributed to terpenes also common to the

24  Mediterranean ecosystem, such as myrcene, terpinolene, linalool, methyl-chavicol and 3-

25  carene (Lee et al., 2006, Bracho-Nunez et al., 2011). We note that all the above-mentioned

26  masses (with the exception of *m/z* 111 and *m/z* 113, for which no rate coefficient was found

27  for the reaction of the unprotonated molecule with OH) have been taken into account in the

28  calculated OH reactivity. The reported time series show that both primary BVOCs and most

29  of the OVOCs resulting from their oxidation had a clear diurnal profile with highest values

30  during midday, similar to that observed for the missing reactivity.

31  Most of the nights were associated with low mixing ratios of BVOCs (29 pptv on average for

32  isoprene) and their oxidation products (40 pptv on average for *m/z* 71) and corresponded to

very low or no missing reactivity. Nevertheless, we note that during some nights (26 to 27, 27 to 28, 29 to 30 July), some compounds ($m/z$ 71, $m/z$ 113) were also present in low amounts and a missing reactivity of about 4 s$^{-1}$ was noticed. These nights were associated with low wind speed and high temperatures that could have favored the accumulation of oxidation products (ratios of $m/z$ 71-to-$m/z$ 69 and nopinone-to-bpinene were maximum 6.4 and 7.7, respectively) as was already observed by night in an oak-forest canopy (Zannoni et al., 2016). The mixing ratios of the first- oxidation products of isoprene and monoterpenes ($m/z$ 71, $m/z$ 139) strongly increased after July 26 when the wind speed was lower and increased again after July 27 when air temperature was also higher. These pieces of evidence also suggest that unmeasured, locally generated BVOC oxidation products contribute significantly to the missing OH reactivity during 27-29 July.

## 5   Conclusions

The total OH reactivity was used in this study to evaluate the completeness of the measurements of reactive trace gases at a coastal receptor site in the western Mediterranean basin during three weeks in summer 2013 (16 July 2013-05 August 2013).

The OH reactivity had a clear diurnal profile and varied with air temperature, suggesting that biogenic compounds were significantly affecting the local atmospheric chemistry. Ancillary trace gases measurements confirmed that most of the daytime reactivity was due to biogenic VOCs, including relevant contributions from oxygenated VOCs, while during nighttime inorganic species and oxygenated VOCs exhibited the largest contribution. The OH reactivity was on average 5±4 s$^{-1}$ (1$\sigma$) with a maximum value of 17±6 s$^{-1}$ (35% uncertainty). The observed maximum is comparable to values of OH reactivity measured at forested locations in northern latitudes (temperate and boreal forests as reported by Di Carlo et al., 2004, Ren et al., 2006, Sinha et al., 2010, Noelscher et al., 2013, Kumar and Sinha 2014, Nakashima et al., 2014). This finding highlights the importance of primary-emitted biogenic VOCs on the OH reactivity, especially where air temperature and solar radiation are high; even though our site was specifically selected for a focused study on mixed and aged continental air masses reaching the basin.

A comparison between the measured OH reactivity and the summed reactivity calculated from the measured species showed that on average 56% of the measured OH reactivity was not explained by the gas measurements during July 23-29. During this period, the air masses came from the West (July 23-27) and the South (July 27-29); lack of pollution events, calm

wind conditions and peaks of air temperature were registered at the field site (28 July). Specifically, during July 27-29 we also detected an increase in oxygenated VOC concentrations originating from the photo-oxidation of primary-emitted BVOCs. Highest yields of these oxidation products ($m/z$ 111, $m/z$ 113, $m/z$ 151) have been attributed to terpenes, which are strongly emitted by Mediterranean ecosystems (Lee et al., 2006, Bracho-Nunez et al., 2011). We found that the missing reactivity was temperature dependent for the same period and such dependency suggests that unmeasured oxidation products of BVOCs, as similarly reported by the study of Mao et al., (2012), caused the missing reactivity.

The impact of biogenic VOCs and their oxidation products is weaker during 23-26 July, since the site received air masses from West, therefore from the marine sector that is less exposed to biogenic emissions. However, large values of missing OH reactivity were also observed, similar to those observed on 27-29 July. The lack of a temperature dependence of the missing reactivity for 23-26 suggests that species other than BVOC oxidation products locally formed were also contributing to the missing OH reactivity.

Mediterranean plants are known to emit large quantities of reactive BVOCs, including sesquiterpenes and oxygenated terpenes (Owen et al., 2001), which were not investigated during our fieldwork. It could be possible that these molecules, as well as their oxidation products, have also played an important role in the missing OH reactivity detected during the campaign.

Further studies with chemical and transport models to identify the important chemical functions of these oxygenated molecules, as well as the effects of long-range transport would be beneficial to provide further insights.

Finally, as the Mediterranean basin differs from side to side, (air masses reception as well as type of ecosystems) more intensive studies at different key spots, e.g. western vs. eastern basin and remote vs. periurban ecosystems, would be helpful for a better understanding of the atmospheric processes linked to the reactive gases over the Mediterranean basin.

# References

Atkinson, R.: Kinetics and mechanisms of the gas-phase reactions of the hydroxyl radical with organic compounds under atmospheric conditions, Chem. Rev. - CHEM REV, 86(1), 69–201, doi:10.1021/cr00071a004, 1986.

Atkinson, R. and Arey, J.: Gas-phase tropospheric chemistry of biogenic volatile organic compounds: a review, Atmos. Environ., 37, 197–219, doi:10.1016/S1352-2310(03)00391-1, 2003.

Atkinson, R., Aschmann, S. M., Winer, A. M., and Carter, W. P. L.: Rate constants for the gas phase reactions of OH radicals and O3 with pyrrole at 295 ± 1 K and atmospheric pressure, Atmospheric Environ. 1967, 18(10), 2105–2107, doi:10.1016/0004-6981(84)90196-3, 1984.

Atkinson, R., Baulch, D. L., Cox, R. A., Crowley, J. N., Hampson, R. F., Hynes, R. G., Jenkin, M. E., Rossi, M. J., and Troe, J.: Evaluated kinetic and photochemical data for atmospheric chemistry: Volume III – gas phase reactions of inorganic halogens, Atmos Chem Phys, 7(4), 981–1191, doi:10.5194/acp-7-981-2007, 2007.

Bracho-Nunez, A., Welter, S., Staudt, M., and Kesselmeier, J.: Plant-specific volatile organic compound emission rates from young and mature leaves of Mediterranean vegetation, J. Geophys. Res.-Atmos., 116, D16304, doi:10.1029/2010JD015521, 2011.

Cappellin, L., Algarra Alarcon, A., Herdlinger-Blatt, I., Sanchez, J., Biasioli, F., Martin, S. T., Loreto, F., and McKinney, K. A.: Field observations of volatile organic compound (VOC) exchange in red oaks, Atmos. Chem. Phys., 17, 4189-4207, doi:10.5194/acp-17-4189-2017, 2017.

ChArMEx project website: http://charmex.lsce.ipsl.fr/, last access on 25/07/2016.

Cuttelod, A., García, N., Abdul Malak, D., Temple, H., and Katariya, V. 2008. The Mediterranean: a biodiversity hotspot under threat. In: J.-C. Vié, C. Hilton-Taylor and S.N. Stuart (eds). The 2008 Review of The IUCN Red List of Threatened Species. IUCN Gland, Switzerland.

Dasgupta, P. K., Dong, S., Hwang, H., Yang, H.-C., and Genfa, Z.: Continuous liquid-phase fluorometry coupled to a diffusion scrubber for the real-time determination of atmospheric formaldehyde, hydrogen peroxide and sulfur dioxide, Atmospheric Environ. 1967, 22(5), 949–963, 1988.

De Gouw, J. and Warneke, C.: Measurements of volatile organic compounds in the earth's atmosphere using proton-transfer-reaction mass spectrometry, Mass Spectrom. Rev., 26(2), 223–257, doi:10.1002/mas.20119, 2007.

Di Carlo, P., Brune, W. H., Martinez, M., Harder, H., Lesher, R., Ren, X., Thornberry, T., Carroll, M. A., Young, V., Shepson, P. B., Riemer, D., Apel, E., and Campbell, C.: Missing OH Reactivity in a Forest: Evidence for Unknown Reactive Biogenic VOCs, Science, 304(5671), 722–725, doi:10.1126/science.1094392, 2004.

Dillon, T. J., Tucceri, M. E., Dulitz, K., Horowitz, A., Vereecken, L., and Crowley, J. N.: Reaction of Hydroxyl Radicals with C4H5N (Pyrrole): Temperature and Pressure Dependent Rate Coefficients, J. Phys. Chem. A, 116(24), 6051–6058, doi:10.1021/jp211241x, 2012.

Draxler, R.R. and Hess, G.D.: An overview of the HYSPLIT_4 modeling system of trajectories, dispersion, and deposition. Aust. Meteor. Mag., 47, 295-308, 1998.

Edwards, P. M., Evans, M. J., Furneaux, K. L., Hopkins, J., Ingham, T., Jones, C., Lee, J. D., Lewis, A. C., Moller, S. J., Stone, D., Whalley, L. K., and Heard, D. E.: OH reactivity in a South East Asian tropical rainforest during the Oxidant and Particle Photochemical Processes (OP3) project, Atmos. Chem. Phys., 13, 9497–9514, doi:10.5194/acp-13-9497-2013, 2013.

Fortems-Cheiney, A., Chevallier, F., Pison, I., Bousquet, P., Saunois, M., Szopa, S., Cressot, C., Kurosu, T.P., Chance, K., and Fried, A. The formaldehyde budget as seen by a global-scale multi-constraint and multi-species inversion system. Atmos. Chem. Phys. *12*, 6699–6721, 2012.

Giorgi, F. and Lionello, P.: Climate change projections for the Mediterranean region, Glob. Planet. Change, 63(2–3), 90–104, doi:10.1016/j.gloplacha.2007.09.005, 2008.

Hansen, R. F., Griffith, S. M., Dusanter, S., Rickly, P. S., Stevens, P. S., Bertman, S. B., Carroll, M. A., Erickson, M. H., Flynn, J. H., Grossberg, N., Jobson, B. T., Lefer, B. L., and Wallace, H. W.: Measurements of total hydroxyl radical reactivity during CABINEX 2009 – Part 1: field measurements, Atmos. Chem. Phys., 14, 2923–2937, doi:10.5194/acp-14-2923-2014, 2014.

Holzinger, R., Lee, A., Paw, K. T., and Goldstein, U. A. H.: Observations of oxidation products above a forest imply biogenic emissions of very reactive compounds, Atmos. Chem. Phys., 5, 67–75, doi:10.5194/acp-5-67-2005, 2005.

Jacob, D.J., Field, B.D., Jin, E.M., Bey, I., Li, Q., Logan, J.A., Yantosca, R.M., and Singh, H.B. Atmospheric budget of acetone. Journal of Geophysical Research: Atmospheres 107, ACH 5–1 – ACH 5–17, 2002.

Jacob, D.J., Field, B.D., Li, Q., Blake, D.R., de Gouw, J., Warneke, C., Hansel, A., Wisthaler, A., Singh, H.B., and Guenther, A. Global budget of methanol: Constraints from atmospheric observations. J. Geophys. Res. *110*, D08303, 2005.

Junkermann, W.: On the distribution of formaldehyde in the western Po-Valley, Italy, during FORMAT 2002/2003, Atmospheric Chem. Phys., 9(23), 9187–9196, 2009.

Kaiser, J., Skog, K. M., Baumann, K., Bertman, S. B., Brown, S. B., Brune, W. H., Crounse, J. D., de Gouw, J. A., Edgerton, E. S., Feiner, P. A., Goldstein, A. H., Koss, A., Misztal, P. K., Nguyen, T. B., Olson, K. F., St. Clair, J. M., Teng, A. P., Toma, S., Wennberg, P. O., Wild, R. J., Zhang, L., and Keutsch, F. N.: Speciation of OH reactivity above the canopy of an isoprene-dominated forest, Atmos. Chem. Phys. Discuss., doi:10.5194/acp-2015-1006, in review, 2016.

Kesselmeier, J. and Staudt, M.: Biogenic Volatile Organic Compounds (VOC): An Overview on Emission, Physiology and Ecology, J. Atmospheric Chem., 33(1), 23–88, doi:10.1023/A:1006127516791, 1999.

Kumar, V. and Sinha, V.: VOC–OHM: A new technique for rapid measurements of ambient total OH reactivity and volatile organic compounds using a single proton transfer reaction mass spectrometer, International Journal of Mass Spectrometry, 374, 55-63, 2014.

Lee, A., A. H. Goldstein, J. H. Kroll, N. L. Ng, V. Varutbangkul, R. C. Flagan, and J. H. Seinfeld: Gas-phase products and secondary aerosol yields from the photooxidation of 16 different terpenes, J. Geophys. Res., 111, D17305, doi:10.1029/2006JD007050, 2006.

Lelieveld, J.: Global Air Pollution Crossroads over the Mediterranean, Science, 298(5594), 794–799, doi:10.1126/science.1075457, 2002.

Levy, H.II: Normal atmosphere: Large radical and formaldehyde concentrations predicted, Science, New series, 173 (3992), 141-143, 1971.

Lindinger, W. and Jordan, A.: Proton-transfer-reaction mass spectrometry (PTR–MS): on-line monitoring of volatile organic compounds at pptv levels, Chem. Soc. Rev., 27(5), 347–375, doi:10.1039/A827347Z, 1998.

Mao, J., Ren, X., Zhang, L., Van Duin, D. M., Cohen, R. C., Park, J.-H., Goldstein, A. H., Paulot, F., Beaver, M. R., Crounse, J. D., Wennberg, P. O., DiGangi, J. P., Henry, S. B., Keutsch, F. N., Park, C., Schade, G. W., Wolfe, G. M., Thornton, J. A., and Brune, W. H.: Insights into hydroxyl measurements and atmospheric oxidation in a California forest, Atmos. Chem. Phys., 12, 8009–8020, doi:10.5194/acp-12-8009-2012, 2012.

Mellouki, A. and Ravishankara, A. R.: Regional Climate Variability and its Impacts in the Mediterranean Area, Springer Science & Business Media., 2007.

Michoud, V., Hansen, R. F., Locoge, N., Stevens, P. S., and Dusanter, S.: Detailed characterizations of the new Mines Douai comparative reactivity method instrument via laboratory experiments and modeling, Atmos. Meas. Tech., 8, 3537-3553, doi:10.5194/amt-8-3537-2015, 2015.

Michoud, V., Sciare, J., Sauvage, S., Dusanter, S., Léonardis, T., Gros, V., Kalogridis, C., Zannoni, N., Féron, A., Petit, J.-E., Crenn, V., Baisnée, D., Sarda-Estève, R., Bonnaire, N., Marchand, N., DeWitt, H. L., Pey, J., Colomb, A., Gheusi, F., Szidat, S., Stavroulas, I., Borbon, A., and Locoge, N.: Organic carbon at a remote site of the western Mediterranean Basin: composition, sources and chemistry during the ChArMEx SOP2 field experiment, Atmos. Chem. Phys. Discuss., doi:10.5194/acp-2016-955, in review, 2017.

Millet, D. B., Guenther, A., Siegel, D. A., Nelson, N. B., Singh, H. B., de Gouw, J. A., Warneke, C., Williams, J., Eerdekens, G., Sinha, V., Karl, T., Flocke, F., Apel, E., Riemer, D. D., Palmer, P. I., and Barkley, M.: Global atmospheric budget of acetaldehyde: 3-D model analysis and constraints from in-situ and satellite observations, Atmos. Chem. Phys., 10, 3405-3425, doi:10.5194/acp-10-3405-2010, 2010.

Misztal, P.K., Hewitt, C.N., Wildt J., Blande, J.D., Eller, A.S.D., Fares, S., Gentner, D.R., Gilman, J.B., Graus, M., Greenberg, J., Guenther, A.B., Hansel, A., Harley, P., Huang, M., Jardine, K., Karl, T., Kaser, L., Keutsch, F.N., Kiendler-Scharr, A., Kleist, E., Lerner, B.M., Li, T., Mak, J., Nölscher, A.C., Schnitzhofer, R., Sinha, V., Thornton, B., Warneke, C., Wegener, F., Werner, C., Williams, J., Worton, D.R., Yassaa, N., and Goldstein A.H.: Atmospheric benzenoid emissions from plants rival those from fossil fuels. *Scientific Reports*. 5:12064. doi:10.1038/srep12064, 2015.

Nakashima, Y., Kato, S., Greenberg, J., Harley, P., Karl, T., Turnipseed, A., Apel, E., Guenther, A., Smith, J., and Kajii, Y.: Total OH reactivity measurements in ambient air in a southern Rocky mountain ponderosa pine forest during BEACHON-SRM08 summer campaign, Atmospheric Environment, 85, 1-8, 2014.

Nash, T.: The colorimetric estimation of formaldehyde by means of the Hantzsch reaction, Biochem. J., 55(3), 416–421, 1953.

Nölscher, A. C., Williams, J., Sinha, V., Custer, T., Song, W., Johnson, A. M., Axinte, R., Bozem, H., Fischer, H., Pouvesle, N., Phillips, G., Crowley, J. N., Rantala, P., Rinne, J., Kulmala, M., Gonzales, D., Valverde-Canossa, J., Vogel, A., Hoffmann, T., Ouwersloot, H. G., Vilà-Guerau de Arellano, J., and Lelieveld, J.: Summertime total OH reactivity measurements from boreal forest during HUMPPA-COPEC 2010, Atmos Chem Phys, 12(17), 8257–8270, doi:10.5194/acp-12-8257-2012, 2012a.

Nölscher, A. C., Sinha, V., Bockisch, S., Klüpfel, T., and Williams, J.: Total OH reactivity measurements using a new fast Gas Chromatographic Photo-Ionization Detector (GC-PID), Atmos Meas Tech, 5(12), 2981–2992, doi:10.5194/amt-5-2981-2012, 2012b.

Nölscher, A. C., Bourtsoukidis, E., Bonn, B., Kesselmeier, J., Lelieveld, J., and Williams, J.: Seasonal measurements of total OH reactivity emission rates from Norway spruce in 2011, Biogeosciences, 10, 4241–4257, doi:10.5194/bg-10-4241-2013, 2013.

Nölscher, A.C., Yañez-Serrano, A.M., Wolff, S., Carioca de Araujo, A., Lavrič, J.V., Kesselmeier, J., and Williams J.: Unexpected seasonality in quantity and composition of Amazon rainforest air reactivity. *Nat. Commun.* 7:10383 doi: 10.1038/ncomms10383, 2016.

Ormeno, E., Fernandez, C., and Mevy, J.P.: Plant coexistence alters terpene emission and content of Mediterranean species, Phytochemistry, 68(6):840-52, 2007.

Owen, S.M., Boissard, C., and Hewitt, C.N.: Volatile organic compounds (VOCs) emitted from 40 Mediterranean plant species: VOC speciation and extrapolation to habitat scale. Atmospheric Environment. 35(32):5393-5409, 10.1016/S1352-2310(01)00302-8, 2001.

Paulot, F., Wunch, D., Crounse, J. D., Toon, G. C., Millet, D. B., DeCarlo, P. F., Vigouroux, C., Deutscher, N. M., González Abad, G., Notholt, J., Warneke, T., Hannigan, J. W., Warneke, C., de Gouw, J. A., Dunlea, E. J., De Mazière, M., Griffith, D. W. T., Bernath, P., Jimenez, J. L., and Wennberg, P. O.: Importance of secondary sources in the atmospheric budgets of formic and acetic acids, Atmos. Chem. Phys., 11, 1989-2013, doi:10.5194/acp-11-1989-2011, 2011.

Preunkert, S., Legrand, M., Pépy, G., Gallée, H., Jones, A., and Jourdain, B.: The atmospheric HCHO budget at Dumont d'Urville (East Antarctica): Contribution of photochemical gas-phase production versus snow emissions, J. Geophys. Res. Atmospheres, 118(23), 13–319, 2013.

Rella, C. W., Chen, H., Andrews, A. E., Filges, A., Gerbig, C., Hatakka, J., Karion, A., Miles, N. L., Richardson, S. J., Steinbacher, M., Sweeney, C., Wastine, B., and Zellweger, C.: High accuracy measurements of dry mole fractions of carbon dioxide and methane in humid air, Atmos. Meas. Tech., 6, 837-860, doi:10.5194/amt-6-837-2013, 2013.

Ren, X., Brune, W. H., Oliger, A., Metcalf, A. R., Simpas, J. B., Shirley, T., Schwab, J. J., Bai, C., Roychowdhury, U., Li, Y., Cai, C., Demerjian, K. L., He, Y., Zhou, X., Gao, H., and

Hou, J.: OH, HO2, and OH reactivity during the PMTACS–NY Whiteface Mountain 2002 campaign: Observations and model comparison, J. Geophys. Res.-Atmos., 111, D10S03, doi:10.1029/2005JD006126, 2006.

Rivera-Rios, J. C., Nguyen, T. B., Crounse, J. D., Jud,W., St. Clair, J.M., Mikoviny, T., Gilman, J. B., Lerner, B. M., Kaiser, J. B., de Gouw, J., Wisthaler, A., Hansel, A., Wennberg, P. O., Seinfeld, J. H., and Keutsch, F. N.: Conversion of hydroperoxides to carbonyls in field and laboratory instrumentation: Observational bias in diagnosing pristine versus anthropogenically controlled atmospheric chemistry, Geophys. Res. Lett., 41, GL061919, doi:10.1002/2014GL061919, 2014.

Sinha, V., Williams, J., Crowley, J. N., and Lelieveld, J.: The Comparative Reactivity Method – a new tool to measure total OH Reactivity in ambient air, Atmos Chem Phys, 8(8), 2213–2227, doi:10.5194/acp-8-2213-2008, 2008.

Sinha, V., Williams, J., Lelieveld, J., Ruuskanen, T. M., Kajos, M. K., Patokoski, J., Hellen, H., Hakola, H., Mogensen, D., Boy, M., Rinne, J., and Kulmala, M.: OH Reactivity Measurements within a Boreal Forest: Evidence for Unknown Reactive Emissions, Environ. Sci. Technol., 44, 6614–6620, doi:10.1021/es101780b, 2010.

Sinha, V., Williams, J., Diesch, J. M., Drewnick, F., Martinez, M., Harder, H., Regelin, E., Kubistin, D., Bozem, H., Hosaynali-Beygi, Z., Fischer, H., Andres-Hernandez, M. D., Kartal, D., Adame, J. A., and Lelieveld, J.: Constraints on instantaneous ozone production rates and regimes during DOMINO derived using in-situ OH reactivity measurements, Atmos. Chem. Phys., 12, 7269–7283, doi:10.5194/acp-12-7269-2012, 2012.

Stein, A.F., Draxler, R.R, Rolph, G.D., Stunder, B.J.B., Cohen, M.D., and Ngan, F.,: NOAA's HYSPLIT atmospheric transport and dispersion modeling system, Bull. Amer. Meteor. Soc., 96, 2059-2077, http://dx.doi.org/10.1175/BAMS-D-14-00110, 2015.

Wallington, T. J.: Kinetics of the gas phase reaction of OH radicals with pyrrole and thiophene, Int. J. Chem. Kinet., 18(4), 487–496, doi:10.1002/kin.550180407, 1986.

Yáñez-Serrano, A. M., Nölscher, A. C., Bourtsoukidis, E., Derstroff, B., Zannoni, N., Gros, V., Lanza, M., Brito, J., Noe, S. M., House, E., Hewitt, C. N., Langford, B., Nemitz, E., Behrendt, T., Williams, J., Artaxo, P., Andreae, M. O., and Kesselmeier, J.: Atmospheric mixing ratios of methyl ethyl ketone (2-butanone) in tropical, boreal, temperate and marine environments, Atmos. Chem. Phys., 16, 10965-10984, doi:10.5194/acp-16-10965-2016, 2016.

Zannoni, N., Dusanter, S., Gros, V., Sarda Esteve, R., Michoud, V., Sinha, V., Locoge, N., and Bonsang, B.: Intercomparison of two comparative reactivity method instruments inf the Mediterranean basin during summer 2013, Atmos. Meas. Tech., 8, 3851-3865, doi:10.5194/amt-8-3851-2015, 2015.

Zannoni, N., Gros, V., Lanza, M., Sarda, R., Bonsang, B., Kalogridis, C., Preunkert, S., Legrand, M., Jambert, C., Boissard, C., and Lathiere, J.: OH reactivity and concentrations of biogenic volatile organic compounds in a Mediterranean forest of downy oak trees, Atmos. Chem. Phys., 16, 1619-1636, doi:10.5194/acp-16-1619-2016, 2016.

Table 1. Measured compounds (whose concentration was above the instrumental detection limits) and their adopted classification in the manuscript for calculating the OH reactivity. Anthropogenic VOCs, BVOCs and OVOCs stand respectively for anthropogenic, biogenic and oxygenated volatile organic compounds.

| Species group | Species name |
|---|---|
| **AVOCs** | methane, ethane, propane, n-butane, n-pentane, n-hexane, n-octane, n-nonane, n-undecane, n-dodecane, 2-methylpentane, 2-methylhexane, 2,2- dimethylbutane, 2,2-dimethylpropane, 2,3- dimethylpentane, 2,4-dimethylpentane, 2,2,3-trimethylbutane, 2,3,4- trimethylpentane, cyclohexane, ethylene, propylene, 1-butene, 2-methyl-2-butene, 3-methyl-1-butene, 1,3-butadiene, *trans*-2-butene, *cis*-2-butene, 1-pentene, *trans*-2-pentene, *cis*-2-pentene, hexene, benzene*[1], toluene*[2], ethylbenzene, styrene, m-xylene, o-xylene, p-xylene*[3], acetylene, 1-butyne, acetonitrile. |
| **BVOCs** | isoprene, a-pinene, b-pinene, d-limonene, a-terpinene, g-terpinene, camphene. |
| **OVOCs** | Acetaldehyde*[4], formic acid*[5], acetone*[6], acetic acid*[7], mglyox, methyl ethyl ketone*[8], propionic acid, ethyl vinyl ketone, butiric acid, nopinone, pinonaldehyde, methacrolein, methyl vinyl ketone, formaldehyde*[9], methanol*[10]. |
| **Others** | NO, NO$_2$, CO. |

*Compounds with anthropogenic and biogenic origin. 1,2,3. Misztal et al., 2015. 4. Millet et al., 2010. 5, 7. Paulot et al., 2011. 6. Jacob et al., 2002. 8. Yanez-Serrano et al., 2016 and Cappelin et al, 2017. 9. Fortems-Cheiney et al., 2012. 10. Jacob et al, 2005.

Table 2. Summary of the experimental methods deployed during the field campaign and needed for calculating the OH reactivity. The number of measured compounds includes the compounds below the instrumental detection limit (LoD).

| Technique | Compounds measured | LoD (pptv) |
|---|---|---|
| PTR-MS | 16 VOCs | 7-500 |
| GC- FID/FID | 43 NMHCs C2-C12 | 10-100 |
| GC-FID/MS | 16 NMHCs (OVOCs+ C3-C7) | 5-100 |
| off-line GC-FID/MS | 35 NMHCs C5-C16 + 5 aldehydes C6-C12 | 5-40 |
| Hantzsch reaction | HCHO | 130 |
| CLD | NOx | 50 |
| WS-CRDS | CO$_2$, CH$_4$, CO | 1000 |

1 Table 3. Relative contributions of individually detected biogenic volatile organic compounds

2 (BVOCs) to the total calculated OH reactivity BVOCs fraction. Daytime BVOCs OH

3 reactivity accounted for a maximum value of 9 s$^{-1}$, on average it was 2±2 s$^{-1}$. Nighttime

4 BVOCs OH reactivity fraction accounted for a maximum value of 0.5 s$^{-1}$, on average it was

5 0.1 s$^{-1}$.

| BVOCs | Day (%) | Night (%) |
|---|---|---|
| a-pinene | 7.7 | 20.7 |
| b-pinene | 16.5 | 16.1 |
| limonene | 12 | 11.4 |
| camphene | 1.5 | 3.1 |
| a-terpinene | 31.1 | 31.3 |
| g-terpinene | 1.3 | 5 |
| isoprene | 30 | 12.5 |

6

7



8 Figure 1. Field site top-view, Corsica, France (42.97°N, 9.38°E, altitude 533 m). Measures: 1.

9 PTR-MS, online and offline chromatography for trace gases analysis; 2. OH reactivity; 3.

10 NO$_x$, O$_3$, aerosols composition and black carbon; 4. Meteo, and particles microphysics; 5.

11 HCHO, trace gases and radicals; 6. CO, CO$_2$, CH$_4$; 7. Trace gases and particle filters; 8.

12 Particles physics. The photo was taken during the installation of the instruments.

13

1   Figure 2. Three-hours averaged data of total OH reactivity measured and calculated from the
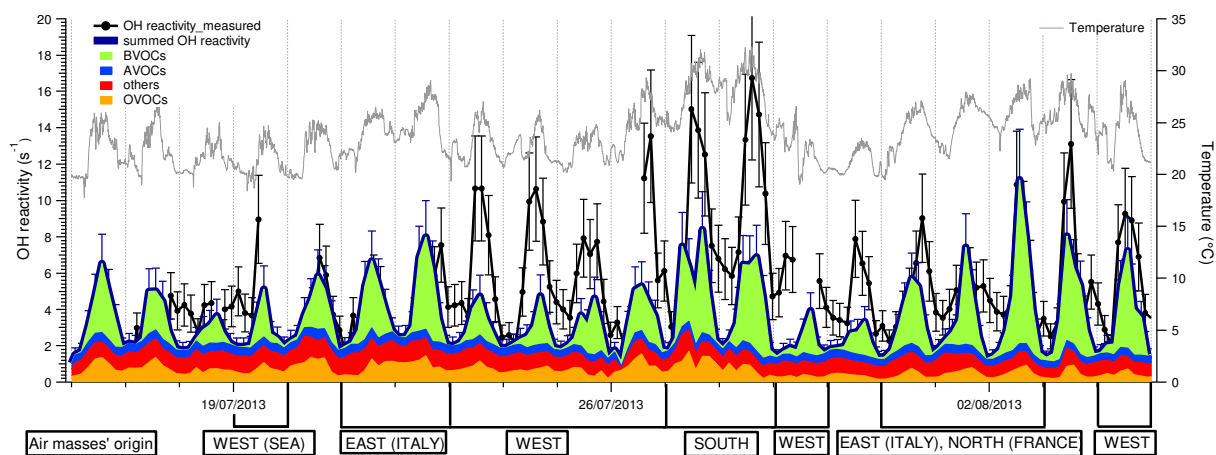
2

3   Figure 2. Three-hours averaged data of total OH reactivity measured and calculated from the

4   measured gases. Summed OH reactivity is represented with the blue thick line and grouped as

5   biogenic VOCs in green, anthropogenic VOCs in blue, oxygenated VOCs in orange and

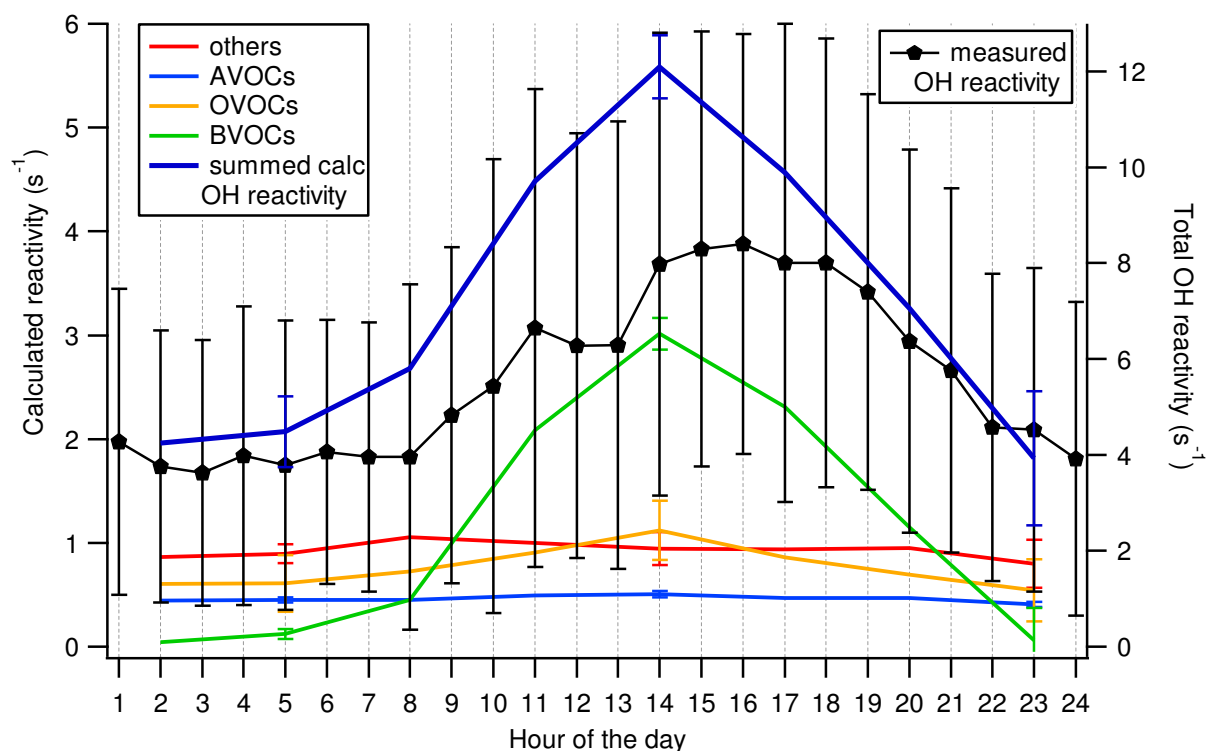6   others in red. Others refer to carbon monoxide (CO) and nitrogen oxides ($NO_x$).



7

8   Figure 3. Diurnal patterns of measured (value with ±1σ, right axis) and calculated OH

9   reactivity (left axis). Others, AVOCs, OVOCs, BVOCs are the contribution of CO and NOx

10  (others), anthropogenic volatiles, oxygenated volatiles and biogenic volatiles to the summed
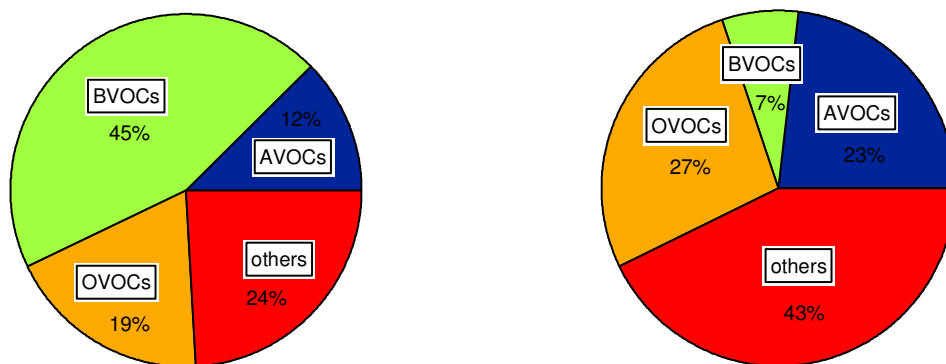
11  calculated OH reactivity.

1

Figure 4. Daytime (left pie) and nighttime (right pie) contributions of the measured compounds to the calculated OH reactivity. Daytime data were collected between 07.30 and 19.30 while nighttime data were between 19.30 and 07.30. Summed OH reactivity during daytime was maximum 11 s$^{-1}$, on average 4±2 s$^{-1}$; while during nighttime it was maximum 3 s$^{-1}$, on average 2±0.4 s$^{-1}$. Biogenic VOCs (green), AVOCs (blue), OVOCs (orange) and others (red) stand for biogenic, anthropogenic, oxygenated volatile organic compounds and carbon monoxide and nitrogen oxides, respectively. During daytime, BVOCs, AVOCs, OVOCs and others contributions were 45%, 12%, 19%, 24%, respectively; while they were 7%, 23%, 27%, 43%, respectively during nighttime.
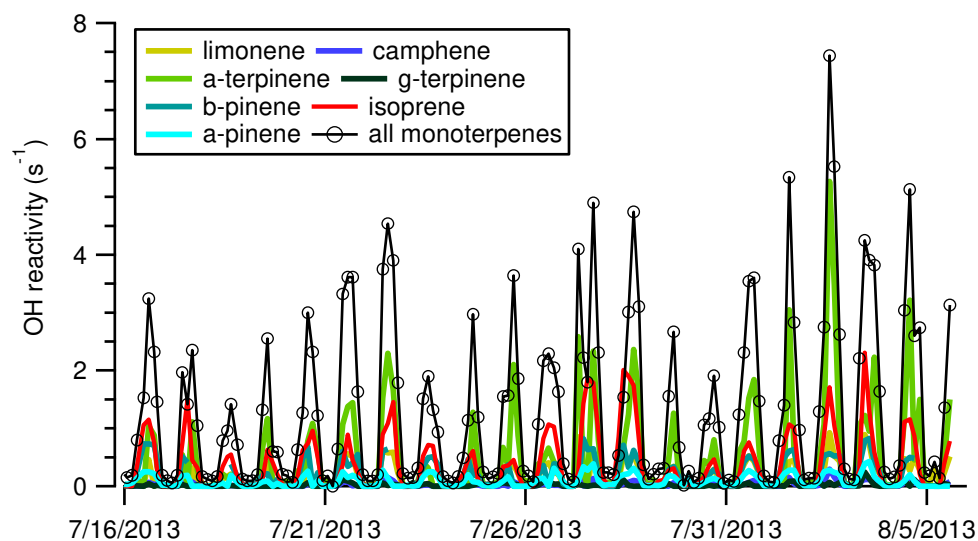


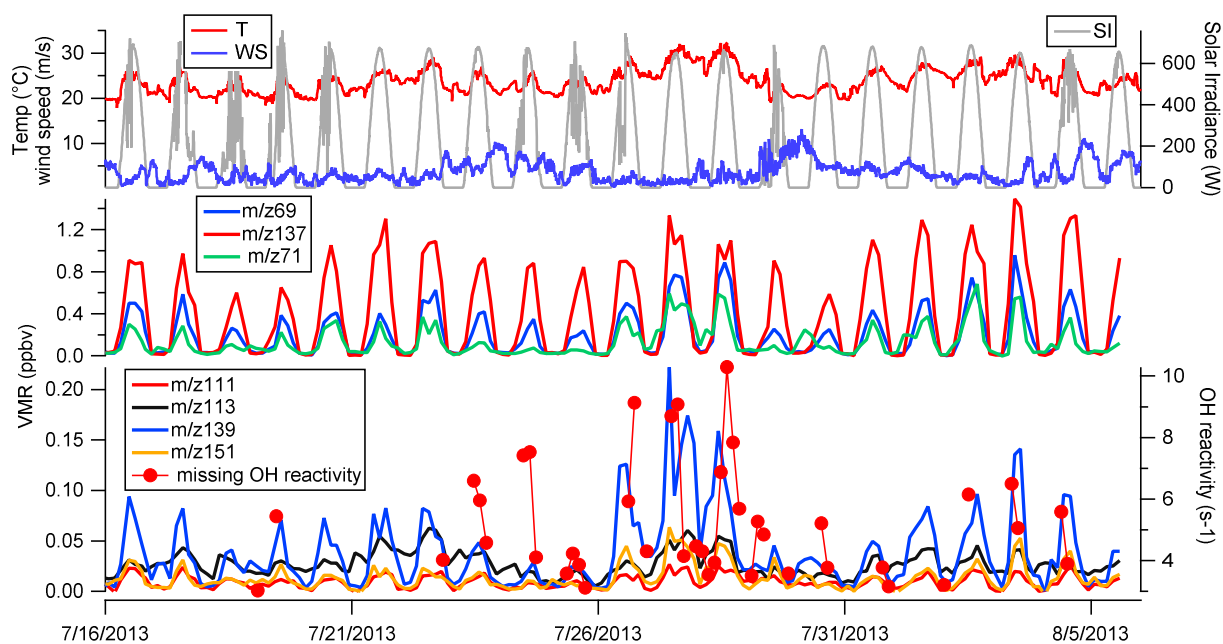Figure 5. Absolute OH reactivity calculated for the measured biogenic compounds.

1

2    Figure 6. Volume mixing ratios (ppbv) of primary-emitted and secondary produced biogenic

3    volatile organic compounds (BVOCs) measured by PTR-MS. Primary emitted BVOCs

4    include: isoprene (*m/z* 69) and monoterpenes (*m/z* 137), oxidation products include: methyl

5    vinyl ketone, methacrolein, possibly isoprene hydroperoxides MVK+MACR+ISOPOOH (*m/z*

6    71), nopinone (*m/z* 139), pinonaldehyde (*m/z* 151), *m/z* 111 and *m/z* 113. Top panel provides

7    data of temperature, wind speed and solar irradiance. The lowest panel shows the variability

8    of the missing OH reactivity, calculated as the difference between measured and calculated

9    reactivity.

10



11
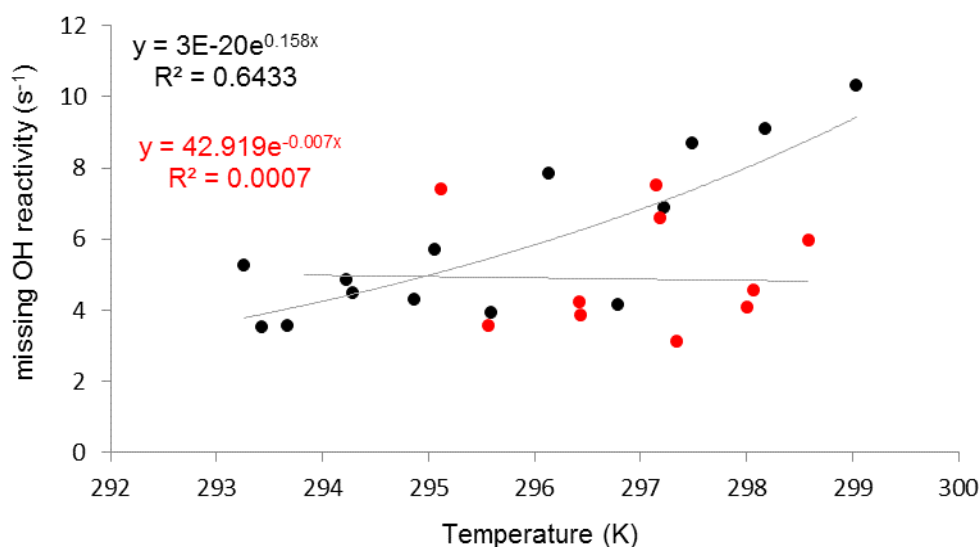
1    Figure 7. The difference between measured and calculated reactivity (missing OH reactivity)

2    during July 23 -26 (red data points) and during July 27 -29 (black data points), dependence to

3    temperature. The missing reactivity is fitted to $E(T)=E(293) \exp(\beta(T-293))$.